文章编号：1001-9014(2023)04-0490-07

DOI:10.11972/j.issn.1001-9014.2023.04.010

Characterization of electrical parameters of high-purity quartz glass in the 40-110 GHz frequency band

ZHU Xiang-Bao[1], SUN Xu[1*], YUE Hai-Kun[2], QIAN Ling-Xuan[1], NI Lei[3]

(1. University of Electronic Science and Technology of China, Chengdu 611731, China;
2. Microsystem & Terahertz Research Center, China Academy of Engineering Physics, Chengdu 610200, China;
3. Key Laboratory of Testing Technology for Manufacturing Process, Southwest University of Science and Technology, Mianyang 621010, China)

Abstract: The transmission line structures such as coplanar waveguide (CPW) and microstrip ring resonator (MRR) were designed on a high-purity quartz substrate (99.9997%) with a thickness of 127 μm. The average insertion loss for the CPW line varied from 0.096 to 0.176 dB/mm in the frequency range of 40-110 GHz. Furthermore, the relative permittivity and loss tangent of the quartz were extracted by the MRR method. The relative permittivity of the quartz substrate in the V-band and W-band ranged with 3.7-3.85 and 3.85-4, respectively. The loss tangent value was approximately 0.004 in the V-band and 0.004-0.006 in the W-band. The performance comparison with other substrates shows that this high-purity quartz has excellent and stable electrical properties and its potential for designing high-performance passive and packaging structures.

Key words: quartz glass, coplanar waveguide, microstrip ring resonator, V-band, W-band

高纯度石英玻璃40~110 GHz频段电参数的表征

朱香宝[1], 孙 旭[1*], 岳海昆[2], 钱凌轩[1], 倪 磊[3]

(1. 电子科技大学,四川 成都 611731;
2. 中国工程物理研究院 微系统与太赫兹研究中心,四川 成都 610200;
3. 西南科技大学 制造过程测试技术教育部重点实验室, 四川 绵阳 621010)

摘要:基于127 μm的高纯度石英(99.999 7%)基底设计了共面波导(CPW)、微带环形谐振器(MRR)结构,通过测试得到在40~110 GHz的频率范围内,CPW线的平均插入损耗在0.096~0.176 dB/mm之间。此外,采用MRR方法提取了石英的相对介电常数和损耗角正切值,该石英基底在V波段和W波段的相对介电常数分别介于3.7~3.85和3.85~4之间,损耗角正切值在V波段约为0.004,在W波段介于0.004~0.006之间。通过与其他基底性能对比表明,该高纯度石英具有良好稳定的电性能,其在设计高性能无源和封装结构方面具有一定的潜力。

关 键 词:石英玻璃;共面波导;微带环形谐振器;V波段;W波段

中图分类号:TN817;TN815　　**文献标识码**:A

Introduction

The development of modern wireless communication technology requires a lot of bandwidth, so the fifth-generation (5G) mobile network has been widely used in everyday life[1]. The performance of 5G networks will be further enhanced by using carrier frequencies in the millimeter wave region, which will achieve higher data rates[2].

However, as more and more high-frequency bands are utilized, numerous new issues arise due to the rapid increase in dielectric substrate loss. For instance, transmission line loss rises as frequency rises; in a similar vein, the dielectric constant of the substrate fluctuates with increasing frequency, causing a significant departure from the design in terms of circuit performance. Sig-

Received date: 2022-09-28, **revised date**: 2023-04-17　　**收稿日期**:2022-09-28,**修回日期**:2023-04-17

Biography: ZHU Xiang-bao (1997-), male, Wuhu, China, master. Research area involves Microwave theory and simulation. E-mail: 202022021934@std.uestc.edu.cn

[*] **Corresponding author**: E-mail: sunxu@uestc.edu.cn

nificant improvements in equipment, packaging techniques, and other areas of the millimeter wave frequency spectrum are necessary to meet these demands[3-5].

The majority of modern millimeter wave packages are comprised of ceramic, fan-out, etc[6-7]. Ceramics are chosen for 5G applications due to their low loss and consistent performance in the millimeter wave spectrum; nevertheless, their expense and integration constraints impede their growth[8]. Fan-out wafer level packaging (FOWLP), which allows for nearly monolithic integration, is becoming more popular. However, it uses compression molding to form rewiring, which can result in significant die shifts. Furthermore, antennas and other high-performance RF structures must be integrated at the top of the module to dissipate heat from the bottom of the chip through silicon pass holes, resulting in a mismatch in the coefficient of thermal expansion (CTE) between the silicon module and the PCB, which can cause reliability issues.

Because of their superior dimensional stability, quartz-based packages are becoming ideal candidates for millimeter wave technology implementation. The CTE of the quartz is customizable, which makes it more compatible with the device structure[9]. For this reason, the basic electrical properties of high-purity quartz (99.9997%) are studied in this paper. The result shows that the quartz has a lower loss tangent and better performance in the high-frequency band, demonstrating the advantages of high-purity quartz packaging in the 5G frequency band.

1 Design of test structures

Coplanar waveguides are frequently used for planar transmission lines, and their insertion loss provides a good indication of a material's aptitude for high-frequency applications. Additionally, a microstrip ring resonator is used to extract the electrical characteristics (dielectric constant and loss tangent) of the quartz substrate in the broadband V-band and W-band.

The bottom of the quartz is covered with a 1 μm thick gold layer as a metal ground in all structural designs, and a 4 μm thick gold layer is subsequently employed to finish the construction of the quartz front, as illustrated in Fig. 1 (a).

1.1 Coplanar waveguide (CPW) lines

The design of CPW is predicated on the quasi-static model of an elliptic integral function subject to conformal transformation[10]. The relationship between the characteristic impedance of CPW, the effective dielectric constant of the substrate and the substrate thickness h, the signal line width W, and the slot spacing g is given by equations (1-4).

$$Z_0 = \frac{60\pi}{\varepsilon_{eff}} \frac{1}{\frac{K(k)}{K(k')} + \frac{K(k_t)}{K(k_t')}} \quad , \quad (1)$$

$$k = \frac{W}{2g + W}, k' = \sqrt{1 - k^2} \quad , \quad (2)$$

$$k_t' = \sqrt{1 - k_t^2}, k_t = \frac{\tan h(\pi W 4h)}{\tan h(\pi(W + 2g)4h)} \quad , \quad (3)$$

$$\varepsilon_{\text{eff}} = \frac{1 + \varepsilon_r \frac{K(k')}{K(k)} \frac{K(k_t)}{K(k_t')}}{1 + \frac{K(k')}{K(k)} \frac{K(k_t)}{K(k_t')}} \quad . \quad (4)$$

In this model, with the increase of h/W, the effective dielectric constant ε_{eff} decreases with the change of g/W. In this paper, we need to extract the effective permittivity and relative permittivity values of the high-purity quartz substrate, so we need ε_{eff} to be as stable as possible when designing the CPW, which is the main direction of concern in our optimization. Furthermore, design optimization should consider the processing process's accuracy, the probe's specification used in the W-band of 100 μm, and the practical requirements for testing the characteristic impedance design of 50 Ω.

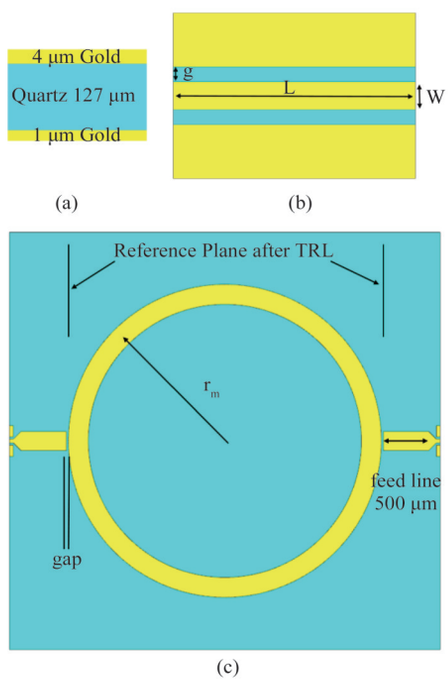

Fig. 1 Test structures, (a) material stack up, (b) CPW line, (c) microstrip ring resonator
图1 测试结构,(a) 材料堆叠,(b) 共面波导线,(c)微带环形谐振器

Based on the above design specifications, the parameters W and g are optimized and simulated, with the simulation results shown in Fig. 2. As can be seen from the figure, the combination of g=25 μm and W=140 μm does not produce resonance and has a lower S_{21}.

The dimensions of the designed CPW are provided in Table 1. Two different lengths of CPW were modeled and designed to characterize the insertion loss per unit length. The structure schematic is shown in Fig. 1 (b).

1.2 Microstrip ring resonator (MRR)

The MRR method is a reliable method for high-frequency dielectric material characterization. The inser-

Table 1 Parameters of the CPW and MRR(μm)
表1 CPW和MRR参数尺寸(μm)

Structure	Parameter	numerical value(μm)
CPW 3 mm CPW 5 mm	*g*	25
	W	140
	L(3 mm)	3 000
	L(5 mm)	5 000
MRR 10 GHz MRR 15 GHz	r_m(10 GHz)	2 700
	r_m(15 GHz)	1 800
	gap	40

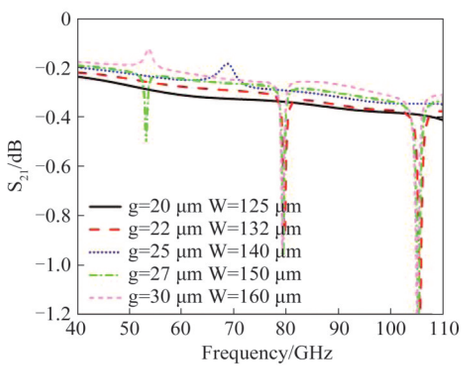

Fig. 2 3 mm CPW line optimization simulation results
图2 3 mm CPW线优化仿真结果

tion loss of the MRR has a resonant period peak. The dielectric constant is calculated using the location of the resonant period peak in the insertion loss of the MRR. And the loss tangent of the material is determined using the resonant peak's no-load quality factor. The desired resonant frequency and the corresponding ring radius are derived from equation (5).

$$f_0 = \frac{nc}{2\pi r_m \sqrt{\varepsilon_{eff}}} \quad , \quad (5)$$

where f_0 is the nth resonant frequency of a ring of average radius r_m, the effective permittivity is ε_{eff}, and c is the speed of light in a vacuum[11-12].

Two MRRs with 10 GHz and 15 GHz fundamental frequencies and Thru-Reflect-Line (TRL) structures were designed to measure multiple resonances in the V and W bands[13]. TRL structures can eliminate the impact of CPW to microstrip transition on the feeder, as well as the impact of the slight impedance mismatch. The response of MRR can be accurately extracted by shifting the measurement reference plane through the TRL structures. Figure 1 (c) depicts a schematic diagram of the MRR's structure.

2 Fabrication

A summary of the fabrication method is provided below. The processing is based on a 127 μm thick quartz substrate.

For the top and bottom metalized layers, the epitaxial growth of the metal layer is first guided by the formation of a seed layer on the quartz surface, followed by the drawing of the photoresist using a designed mask and the formation of the desired metal pattern using lithography techniques. Eventually, the photoresist is removed and the seed layer is etched to obtain the desired structure. The manufactured test structure is depicted in Fig. 3, both CPW lines and MRR structures are processed on the quartz front with a metal thickness of 4 μm, and the quartz back is entirely covered with a metal thickness of 1 μm.

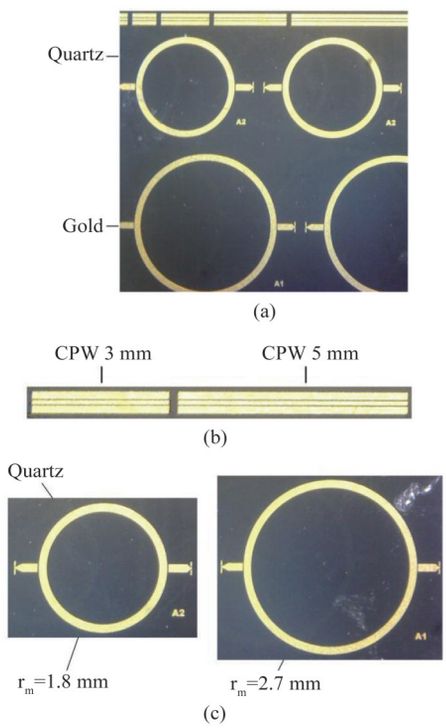

Fig. 3 Fabricated test structure, (a) partial samples, (b) CPW line, (c) microstrip ring resonator
图3 制备的测试结构,(a) 部分样片, (b) 共面波导线, (c) 微带环形谐振器

3 Measurement and analysis

The measurement setup shown in Fig. 4 employs a probe stage to test the generated and processed samples. For accurate calibration, the frequency step change is 0.1 GHz across the whole frequency range of the test.

3.1 Coplanar waveguide (CPW) lines

Multiple identical structures processed in the same batch were tested to ensure the accuracy of the test data. Figure 5 shows the results of fabricating and measuring two different lengths of CPW (3 mm and 5 mm). The reflection coefficients in Fig. 5 are generally less than -10 dB, which indicates good impedance matching. Because the sample structure tested was a thin-film circuit processed on a 2-inch quartz wafer, there would be some processing deviation of the graphic structure at different positions on the wafer. This also resulted in a slight difference in the test results, with the S_{21}'s difference within the acceptable range of 0.2 dB.

The S_{21} per unit length (dB/mm) is shown in Fig. 6. The insertion loss for CPW lines varies from 0.096 to

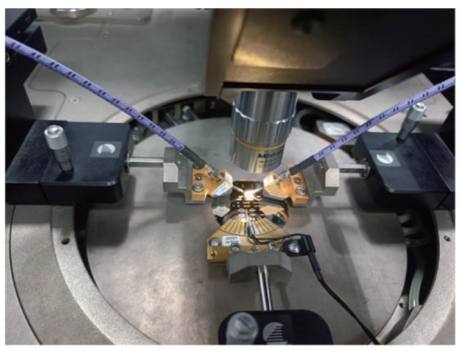

(a)

(b)

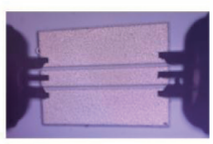

(c)

Fig. 4 The schematic diagram of the test device, (a) measurement setup, (b) sample ready to be probed, (c) measurements underway
图4 测试装置示意图,(a) 测试设置,(b) 样品准备测试,(c) 进行测试

0.176 dB/mm in the frequency range of 40-110 GHz. According to the data in Fig. 6, the insertion loss of the CPW line on the quartz substrate at 40 GHz, 77 GHz, and 110 GHz is 0.096 dB/mm, 0.125 dB/mm, and 0.176 dB/mm, respectively.

At the same time, the average insertion loss of the high-purity quartz-based transmission line has been compared with the performance of other high-frequency material transmission lines, such as ABF/glass/ABF[14], Rogers RT Duriod 6002[15], and LCP materials[16] in the frequency region from 40 to 110 GHz.

As can be seen from Table 2, the test results are slightly better than some high-frequency materials, which indicates the good transmission performance of the high-purity quartz. In addition, quartz material can support high wiring density, excellent assembly spacing, and other advantages, and the quartz thermal expansion coefficient is customizable, which makes it more compatible with device structures.

3.2 Microstrip ring resonator (MRR)

MRRs with two resonant frequencies (10 GHz and 15 GHz) were designed to avoid characterization errors caused by manufacturing and measurement errors. The measured results for multiple samples are shown in Fig. 7. Sharp resonances have been captured across the frequency region.

Since the dispersion of the microstrip line is prominent at high frequency, the dispersion model is adopted to extract the effective permittivity value from the resonant frequency of S_{21} of the MRR, and then calculate the relative permittivity according to the extracted effective permittivity value[17].

For the MRR, the effective permittivity can be obtained from Equation (6).

$$\varepsilon_{\text{eff}} = \left(\frac{nc}{2\pi r_m f_0}\right)^2 \quad , \quad (6)$$

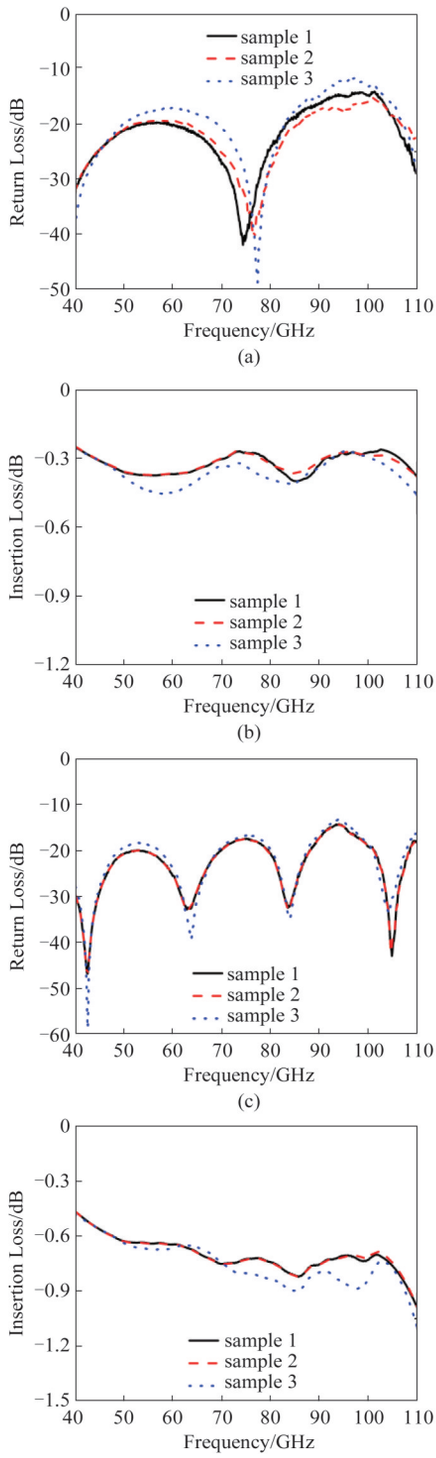

Fig. 5 Measured S-parameter of CPW lines, (a) S_{11} measured value of 3 mm CPW line, (b) S_{21} measured value of 3 mm CPW line, (c) S_{11} measured value of 5 mm CPW line, (d) S_{21} measured value of 5 mm CPW line
图5 共面波导线S参数测量值,(a) 3 mm CPW线的 S_{11} 测量值,(b) 3 mm CPW线的 S_{21} 测量值, (c) 5 mm CPW线的 S_{11} 测量值,(d) 5 mm CPW线的 S_{21} 测量值

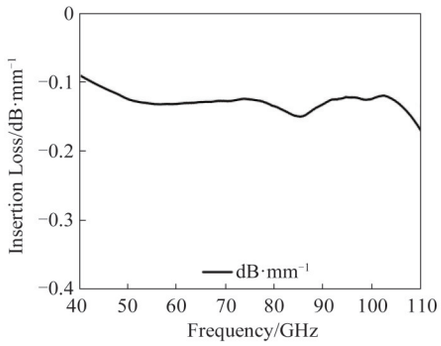

Fig. 6 S_{21} (dB/mm) per unit length
图6 单位长度的 S_{21} (dB/mm) 值

Table 2 Comparison of the performance of quartz-based transmission lines with other high-frequency materials (dB/mm)
表2 石英基传输线与其他高频材料性能比较(dB/mm)

	40 GHz	60 GHz	77 GHz	110 GHz
LCP	NA	0.15	0.175	0.225
ABF/glass/ABF	0.095	0.12	0.17	0.25
Rogers	0.075	0.10	0.13	NA
Quartz (this work)	0.096	0.111	0.125	0.176

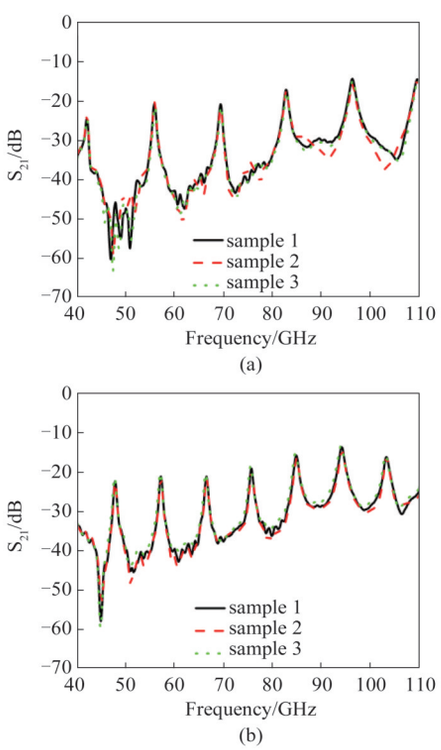

Fig. 7 Measured S_{21} response of microstrip ring resonator, (a) r=1.8 mm(15 GHz), (b) r=2.7 mm(10 GHz)
图7 微带环形谐振器 S_{21} 测量值,(a) r=1.8 mm(15 GHz),(b) r=2.7 mm(10 GHz)

where f_0 is the nth resonant frequency of a ring of average radius r_m, ε_{eff} is the effective permittivity, and c is the speed of light in a vacuum.

As shown in Equation (7), the relative permittivity of quartz can be calculated using the effective permittivity and the size of the microstrip line.

$$\varepsilon_r = \frac{2\varepsilon_{eff} + M - 1}{M + 1} \quad , \quad (7)$$

where $M = (1+12h/W_{eff})^{-1/2}$, W_{eff} is the effective strip width accounting for the nonzero strip thickness, $W_{eff} = W+(t/h)\times[\ln(2h/t)+1]$, h is the thickness of the quartz substrate, t and W are the physical thickness and width of the gold conductor.

Figure 8 displays the relative permittivity that is obtained from the extraction. The vertical bars represent a confidence interval of 95%. It can be seen that the quartz substrate's dielectric constant is stable in the V-band between 3.7 and 3.85 and in the W-band between 3.85 and 4, indicating that the quartz substrate's dielectric constant is relatively stable in both bands.

The dielectric loss[18] is calculated using the ring resonator method by subtracting the theoretical conductor loss value from the total loss at each resonant peak's frequency location.

$$\alpha_d = \alpha_{total} - \alpha_c \quad , \quad (8)$$

where α_{total} is the total loss, α_c is the conductor loss, and α_d is the dielectric loss.

Then the loss tangent $\tan\delta$ is obtained by substituting α_d into the following equation (9).

$$\tan\delta = \frac{\alpha_d \lambda_0 \sqrt{\varepsilon_{eff}}\,(\varepsilon_r - 1)}{\pi\varepsilon_r(\varepsilon_{eff} - 1)} \quad , \quad (9)$$

where λ_0 is the free-space wavelength, ε_{eff} is the effective

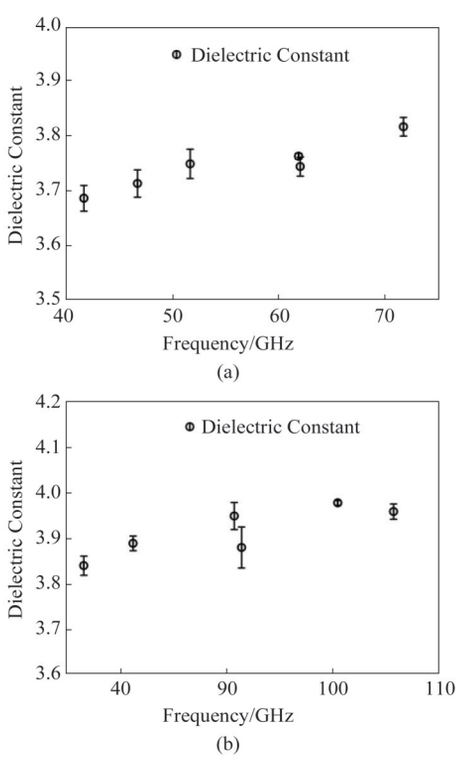

Fig. 8 Dielectric constant of extracted quartz substrate, (a) V-band, (b) W-band
图8 提取的石英基板介电常数,(a) V波段,(b) W波段

dielectric constant, and ε_r is the relative dielectric constant.

According to Fig. 9, which depicts the extracted loss tangent, the loss tangent is around 0.004 in the V-band and increases slightly between 0.004 and 0.006 in the W-band. The vertical bars represent a confidence interval of 95%.

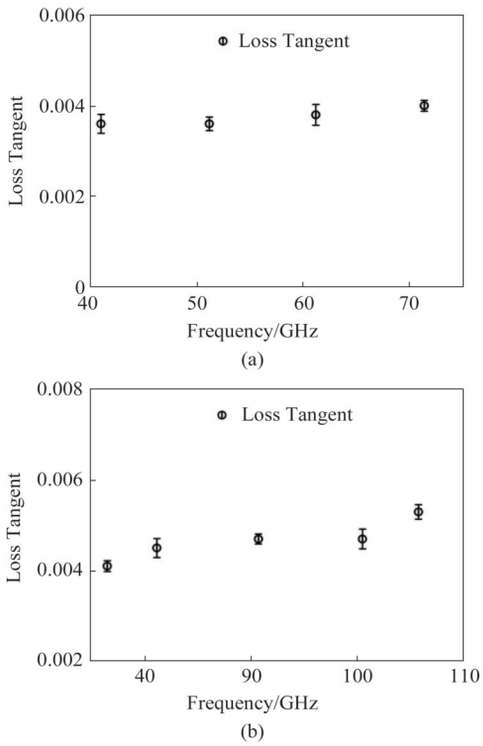

Fig. 9 Loss tangent of extracted quartz substrate, (a) V-band, (b) W-band
图9 提取的石英基板损耗角正切,(a) V波段,(b) W波段

Table 3 is the comparison between the extracted loss tangent and other high-frequency stacking materials, such as ABF/glass/ABF[13] and ZIF/glass/ZIF[8]. It can be seen from the table that the loss tangent of the high-purity quartz substrate is lower and more stable in the frequency range.

Table 3 Comparison of the loss tangent of the extracted quartz base with other high-frequency materials
表3 提取的石英基板损耗正切与其他高频材料比较

ABF/glass/ABF	ZIF/glass/ZIF	Quartz(this work)
0.004-0.006(20-60 GHz)	0.012(50 GHz)	~0.004(40-75 GHz)
0.007-0.015(75-163 GHz)	NA	0.004-0.006(75-110 GHz)

4 Conclusion

The microstrip ring resonant cavity method is used in this paper to characterize the transmission lines on quartz and extract the dielectric properties of the quartz material. The extracted relative permittivity is stable in the V-band range of 3.7-3.85 and the W-band range of 3.85-4. The extracted loss tangent values in the V-band are around 0.004 and between 0.004 and 0.006 in the W-band, the extracted results are obtained with 95% confidence intervals to account for any uncertainty due to process accuracy and measurement errors. The results show that the quartz substrate has stable electrical properties and low-loss tangents at high frequencies. In addition, the loss of conductors for coplanar waves is designed and evaluated. The average insertion loss for CPW lines varies from 0.096 to 0.176 dB/mm in the frequency range of 40-110 GHz. The excellent performance of the transmission lines demonstrates that a highly effective millimeter-wave circuit/device design is feasible on quartz substrates in the V-band and the W-band. This work investigates high-purity quartz substrates (99.999 7%) in the 40-110 GHz frequency band. It supports the option of systematic packaging on an inexpensive thin quartz substrate.

References

[1] T. S. Rappaport, Yunchou Xing, Ojas Kanhere, *et al*. Wireless Communications and Applications Above 100 GHz: Opportunities and Challenges for 6G and Beyond [J]. *IEEE Access*, 2019, **7**: 78729-78757.
[2] M. Agiwal, A. Roy, N. Saxena, *et al*. Next generation 5G wireless networks: A comprehensive survey [J]. *IEEE Communications Surveys & Tutorials*, 2016, **18**(3): 1617 - 1655.
[3] Dielacher F, Tiebout M, Lachner R, *et al*. SiGe BiCMOS technology and circuits for active safety systems [C]. 2014 International Symposium on VLSI Technology, Systems and Application (VLSI-TSA), Hsinchu, Taiwan, China, 2014: 1-4.
[4] Wagner C, Böck J, Wojnowski M, *et al*. A 77 GHz automotive radar receiver in a wafer level package [C]. 2012 IEEE Radio Frequency Integrated Circuits Symposium, Montreal, QC, Canada, 2012: 511-514.
[5] Khan W T, Sitaraman S, Vera A L, *et al*. A V-band end-fire Yagi-Uda antenna on an ultra-thin glass packaging technology [C]. 2015 European Microwave Conference (EuMC), Paris, France, 2015: 618-621.
[6] M. Swaminathan, V. Sundaram, J. Papapolymerou, *et al*. Polymers for RF Apps [J]. *IEEE Microwave Magazine*, 2011, **12**(7): 62-77.
[7] M. u. Rehman, S. Ravichandran, S. Erdogan, *et al*. W-band and D-band Transmission Lines on Glass Based Substrates for Sub-THz Modules [C]. 2020 IEEE 70th Electronic Components and Technology Conference (ECTC), Orlando, FL, USA, 2020: 660-665.
[8] Khan W T, Tong J, Sitaraman S, *et al*. Characterization of electrical properties of glass and transmission lines on thin glass up to 50 GHz [C]. 2015 IEEE 65th Electronic Components and Technology Conference (ECTC), San Diego, CA, USA, 2015: 2138-2143.
[9] Tong J, Sundaram V, Shorey A, *et al*. Substrate-integrated waveguides in glass interposers with through-package-vias [C]. 2015 IEEE 65th Electronic Components and Technology Conference (ECTC), San Diego, CA, USA, 2015: 2222-2227.
[10] David M Pozar. Microwave Engineering [M]. Beijing: Publishing House of Electronics Industry (David M Pozar. 微波工程. 北京:电子工业出版社), 2019.
[11] Hsieh L H, Kai C. Equivalent lumped elements G, L, C, and unloaded Q's of closed- and open-loop ring resonators [J]. *IEEE Transactions on Microwave Theory and Techniques*, 2002, **50**(2): 453-460.
[12] Wolff I, Knoppik N. Microstrip ring resonator and dispersion measurement on microstrip lines [J]. *Electronics Letters*, 1971, **7**(26): 779-781.
[13] Marks R B. A multiline method of network analyzer calibration [J]. *IEEE Transactions on Microwave Theory and Techniques*, 1991, **39**(7): 1205-1215.
[14] M. ur Rehman, S. Ravichandran, A. O. Watanabe, *et al*. Characterization of ABF/Glass/ABF Substrates for mmWaveApplications [J]. *IEEE Transactions on Components, Packaging and Manufacturing Technology*, 2021, **11**(3): 384-394.

[15] F. Fesharaki, T. Djerafi, M. Chaker, *et al*. Guided-wave properties of mode-selective transmission line [J]. *IEEE Access*, 2018, **6**: 5379 - 5392.

[16] D. Thompson, P. Kirby, J. Papapolymeron, *et al*. W-band characterization of finite ground coplanar transmission lines on liquid crystal polymer (LCP) substrates [C]. 2003 53rd Electronic Components and Technology Conference, New Orleans, LA, USA, 2003: 1652 - 1655.

[17] Kirschning M, Jansen R H. Jansen. Accurate model for effective dielectric constant of microstrip with validity up to mm-wave frequencies [J]. *Electronics Letters*, 1982, **18**(6): 272-273.

[18] Gang Zou, H. Gronqvist, J. P. Starski, *et al*. Characterization of liquid crystal polymer for high frequency system-in-a-package applications [J]. *IEEE Transactions on Advanced Packaging*, 2002, **50** (4): 503-508.